EUROPEAN ORGANIZATION FOR NUCLEAR RESEARCH
European Laboratory for Particle Physics

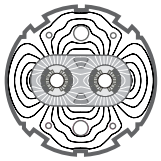

LHC Project Note 362

2005-02-02
Andy.Presland@cern.ch
Brennan.Goddard@cern.ch

Performance of the TCDQ diluter system

A.Presland, B.Goddard

Keywords: beam dump, extraction, protection, collimation, diluter, halo, quench

Summary

A single sided mobile graphite diluter block TCDQ, in combination with a two-sided secondary collimator TCS and an iron shield TCDQM, will be installed in front of the superconducting quadrupole Q4 magnets in IR6, in order to protect it and other downstream LHC machine elements from destruction in the event of a beam dump that is not synchronised with the abort gap. The TCDQ and associated elements should also intercept spurious particles in the beam abort gap to prevent quenches from occurring during regular beam aborts, and must also intercept the particles from the secondary halo during low beam lifetime without provoking quenches. In this note the conceptual design of the TCDQ system is briefly presented, with the load conditions and performance criteria. The FLUKA energy deposition simulations are described, and the results discussed in the context of the expected performance levels for LHC operation, in particular for the problems associated with quenching the downstream superconducting Q4 magnet. Options for improvement are elucidated and required future work is defined.

1. INTRODUCTION

The LHC beam dumping system [1] includes a fast-pulsed kicker magnet system MKD, which deflects the beam horizontally into to a set of Lambertson septum magnets MSD. These deflect the beam vertically out of the LHC machine into the TDE dump absorber block. A single sided mobile diluter block TCDQ, in combination with a secondary collimator TCS and an iron shield TCDQM [2], will be installed in front of the superconducting quadrupole Q4 magnet in IR6, in order to protect it and other LHC machine elements from destruction in the event of a beam dump that is not synchronised with the abort gap [3].

The TCDQ element should protect the LHC from damage from swept bunches under all conditions, in particular the arc aperture at 450 GeV and the low-beta triplet aperture at 7 TeV.

The TCDQ must also prevent quenches of Q4, arising from spurious particles in the abort gap during a normal beam dump, and from particles lost from the beam halo during regular operation.

For compatibility reasons, and to improve the positioning tolerance significantly, a double-sided TCS collimator will be installed after the TCDQ to precisely define the horizontal beam position and to achieve higher precision collimation of secondary halo particles from both

sides. The TCS will receive a potentially high load from the secondary halo in the event of low beam lifetime.

Figure 1 shows a schematic presentation of the layout and function of the TCDQ diluter element, with the TCS and TCDQM.

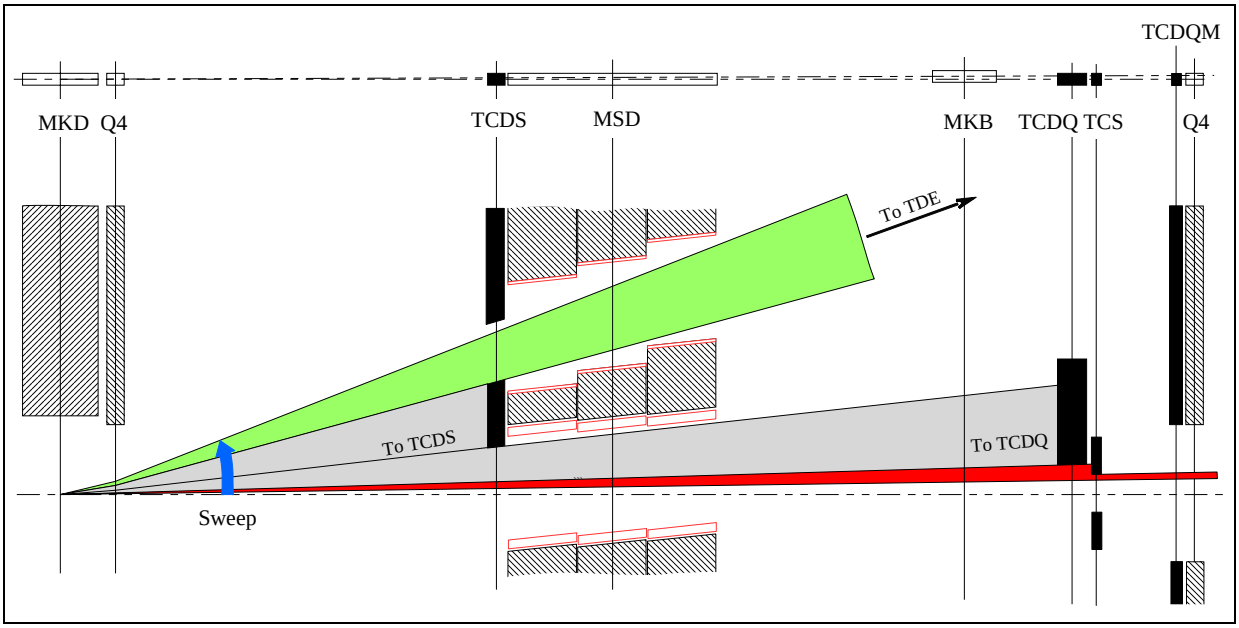

Figure 1. Schematic and functional layout of TCDQ, TCS and TCDQM elements in IR6 (one beam).

2. MAIN DESIGN FEATURES OF TCDQ, TCS AND TCDQM

The full details of the TCDQ conceptual design can be found in [2]. Considering the ultimate LHC beam intensity and the total number of bunches in case of a MKD sweep, several scenarios have been studied [4] for the configuration of the TCDQ. A 6.0 m single-sided graphite or CFC absorber block (density ~1.7 g/cm^3), positioned at ~12.5 m in front of the Q4 magnet, followed by a 2.1 m iron TCDQM mask (density 7.9 g/cm^3) positioned directly in front of the Q4 magnet, as shown schematically in Figures 2 and 3, has shown to give the best results. Presently the TCDQM inner diameter is assumed to be 70 mm, the same as the MQY coil aperture.

In addition to the single-sided TCDQ, a short two-sided TCS element is proposed. This will be set at a slightly (~1 σ) closer setting than the TCDQ proper, and will intercept the secondary halo, as do the TCS collimators in the collimation insertions. This provision allows a relaxation of the tolerances for the TCDQ, and eases the design as regards cooling and radiation dose. It will also provide a real definition of the beam position between the jaws, helping to avoid problems with positioning the TCDQ long jaw relative to the beam.

Clearly, the TCS must survive the swept beam case, and scattered particles from the TCS jaws must not quench Q4.

For practical reasons, the TCDQ will be composed of two vacuum tanks, identical to the TCDS design, and to accommodate the 6 m jaw length, a total length of 6.85 metres is required for the complete TCDQ structure. The TCDQ jaw needs to be motorised and due to the considerable length of the structure in a reduced space, an accurate positioning of the collimator jaw at 450

GeV and 7 TeV can only be achieved by moving the complete vacuum tanks. The required settings of the TCS and TCDQ at 450 GeV and 7 TeV are shown in Table 1.

Table 1. Beam sizes and nominal TCS and TCDQ settings at 450 GeV and 7 TeV.

	450 GeV	**7 TeV**
Beam size σ [h/v]	2.0 / 1.2 mm	0.51 / 0.3 mm
TCS setting	7 σ / 14.1 mm	9 σ / 4.6 mm
TCDQ setting	8 σ / 16.1 mm	10 σ / 5.1 mm

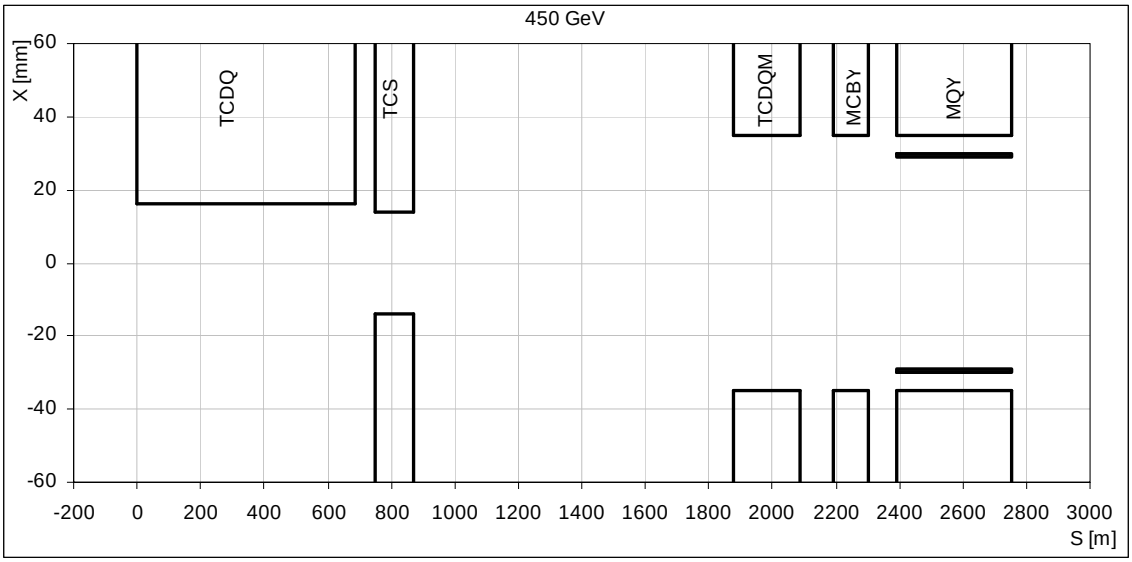

Figure 2. Schematic layout at 450 GeV of TCDQ, TCS and TCDQM, with MCBY and MQY.

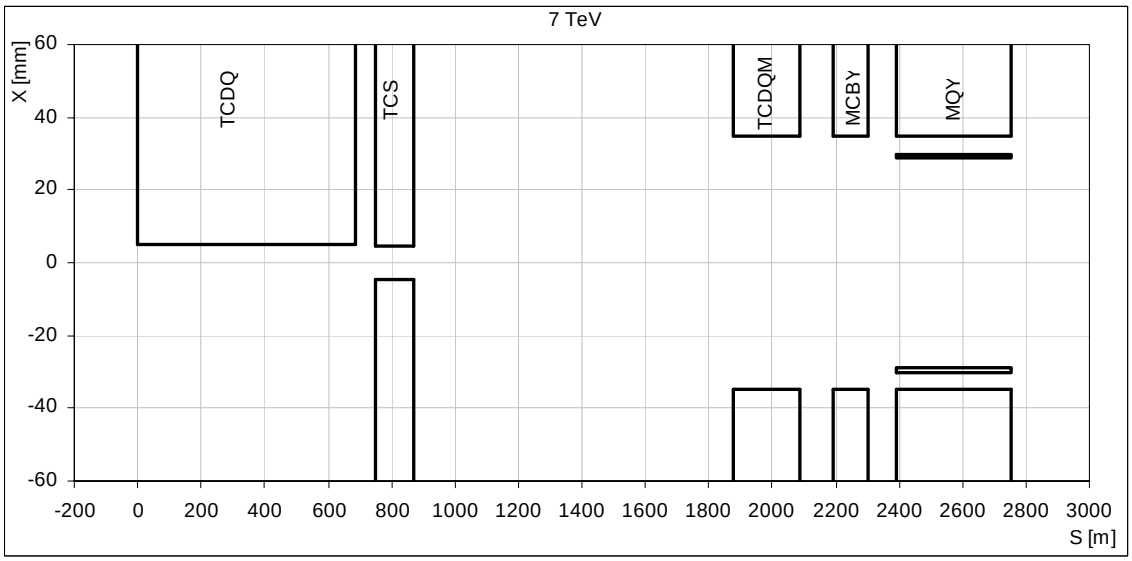

Figure 3. Schematic layout at 7 TeV of TCDQ, TCS and TCDQM, with MCBY and MQY.

3. PERFORMANCE CRITERIA AND LOAD ASSUMPTIONS

The performance criteria of the TCDQ system depend on the damage and quench limits of the downstream superconducting magnets. These quench and damage limits are not specifically available for the MQY magnets; best estimates for the various figures of merit have been gathered together, Table 2.

Table 2. Assumed limits for the superconducting elements MCBY and MQY (Q4)

Limit	**450 GeV**	**7 TeV**
Damage; instantaneous deposition [5]	87 J/cm^3	87 J/cm^3
Quench; instantaneous deposition [6]	35 mJ/cm^3	4 mJ/cm^3
Quench; localised DC deposition [7]	1 - 10 mW/cm^3	0.2 - 5 mW/cm^3
Quench; total magnet power deposition [8]	34 W	34 W

3.1. Protection from asynchronous beam abort

3.1.1. Protection of Q4 at 7 TeV

In the event of an unsynchronised beam abort, generated by one MKD magnet pre-trigger followed by re-triggering of the remaining 14 magnets 1.2 μs later, the TCDQ will intercept ~36 proton bunches at 7 TeV. With an ultimate intensity of 1.7 10^{11} protons per bunch, the transverse intensity profile is as shown in Figure 4. For this load case the energy deposited in the MCBY and MQY should not exceed the damage limit.

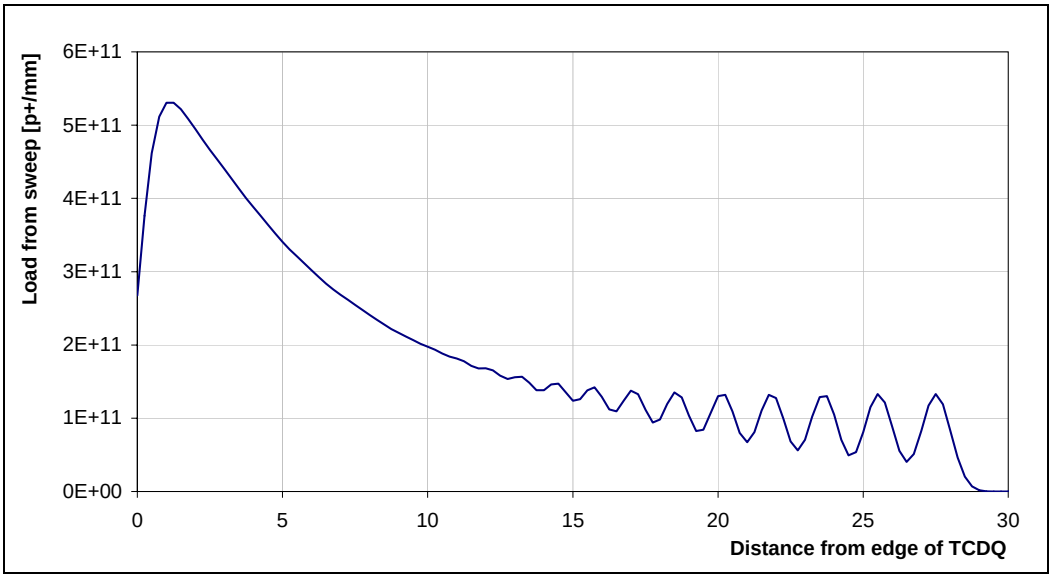

Figure 4 – Asynchronous dump – intensity profile on TCDQ/TCS at 7 TeV arising from an MKD pre-trigger followed by re-triggering of the remaining 14 magnets 1.2 μs later (LHC optics V6.5). 36 ultimate bunches are superimposed.

3.1.2 Protection of the LHC arc at 450 GeV

At 450 GeV the LHC arc has a transverse aperture of about 7.5 σ [9], meaning that the TCDQ protection system will need to have a similar transverse setting (~15 mm). The TCS is presently assumed to be set at 7 σ, the TCDQ at 8 σ.

To protect aperture limits downstream of the TCDQ, the system should reduce the intensity of the primary beam to a safe level, which for the nominal emittance is approximately $2\ 10^{12}$ p+ or a reduction by a factor of 250. This requires only about 2.5 m of graphite with an interaction length of ~46 cm [10]; the 6 m TCDQ is thus already largely sufficient. The TCS/TCDQ must be positioned with respect to the beam with an accuracy of ±0.5 σ.

3.1.3 Protection of the low-β triplets at 7 TeV

The low-β triplets have a transverse aperture of about 10 σ for squeezed optics [9]. The TCS is assumed to be set at 9 σ, the TCDQ at 10 σ.

To protect the low-β triplets, the system should reduce the intensity of the primary beam by a factor of 50,000. This requires 5 m of graphite [10], so the 6 m TCDQ is sufficient. Again, the TCS/TCDQ must be positioned with respect to the beam with an accuracy of ±0.5 σ.

3.2 Quench protection of Q4 from secondary beam halo

The tight settings of the TCDQ mean that the system could intercept a significant continuous beam load from the secondary halo. The TCDQ system must be able to protect the machine at the settings described above, while not producing a quench in the Q4 due to this continuous load. The maximum and integrated power deposition in the superconducting coils should not exceed the quench limits given in table 2. The secondary halo form is shown in Figures 5 and 6 [11]. For the minimum lifetime, a total of about $6\ 10^{11}$ p+ / s are assumed lost. The maximum number which could impact the TCS/TCDQ is this number multiplied by the cleaning inefficiency for the transverse setting of the jaw, to give the total loads shown in Table 3.

Table 3. Assumed worst-case halo total beam loads for TCS and TCDQ.

	450 GeV	**7 TeV**
Load on TCS [p+ / s]	$1.3\ 10^{11}$	$7.5\ 10^{8}$
Load on TCDQ [p+ / s]	$6\ 10^{9}$	$4.5\ 10^{8}$

The load distributions shown in Figures 5 and 6 were then approximated with rectangular load profiles for the FLUKA energy deposition simulations, as shown in Figures 7 and 8. Note that the load is assumed to be shared equally to the left and right of the beam axis, such that the TCDQ intercepts part of the halo to one side only, with the TCS jaws intercepting the remainder.

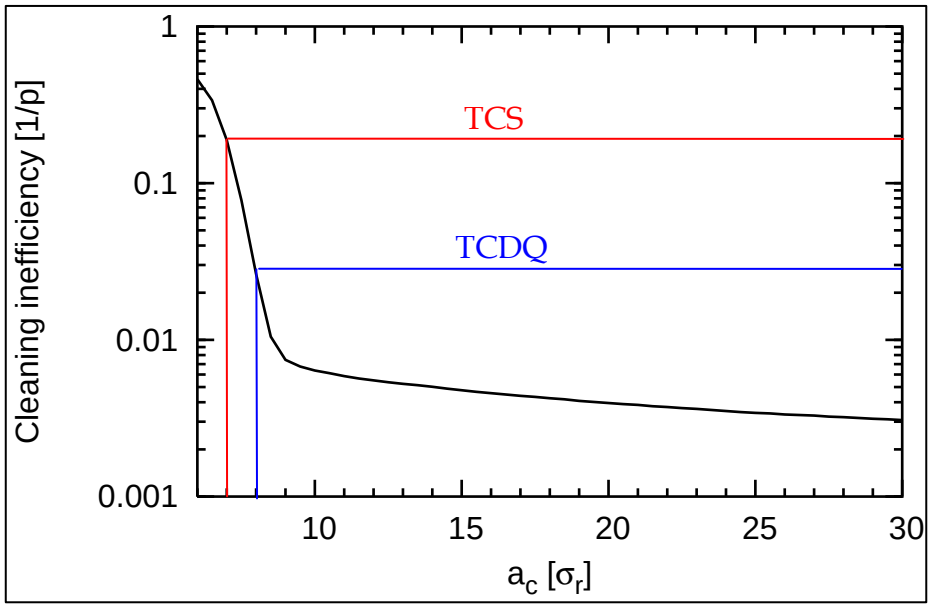

Figure 5. Secondary halo profile at 450 GeV, showing TCS (7 σ) and TCDQ (8 σ) positions.

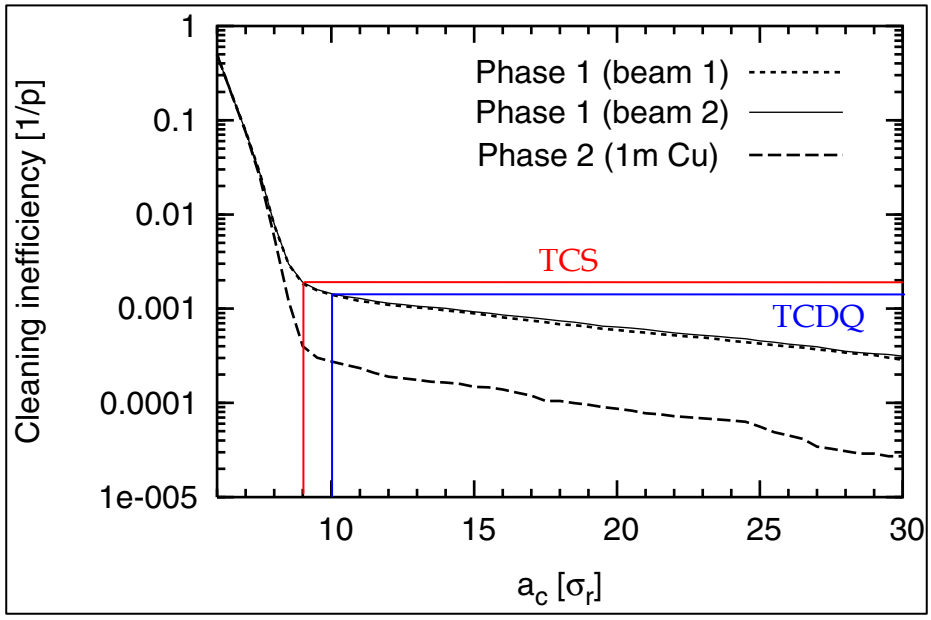

Figure 6. Secondary halo profile at 7 TeV, showing TCS (9 σ) and TCDQ (10 σ) positions.

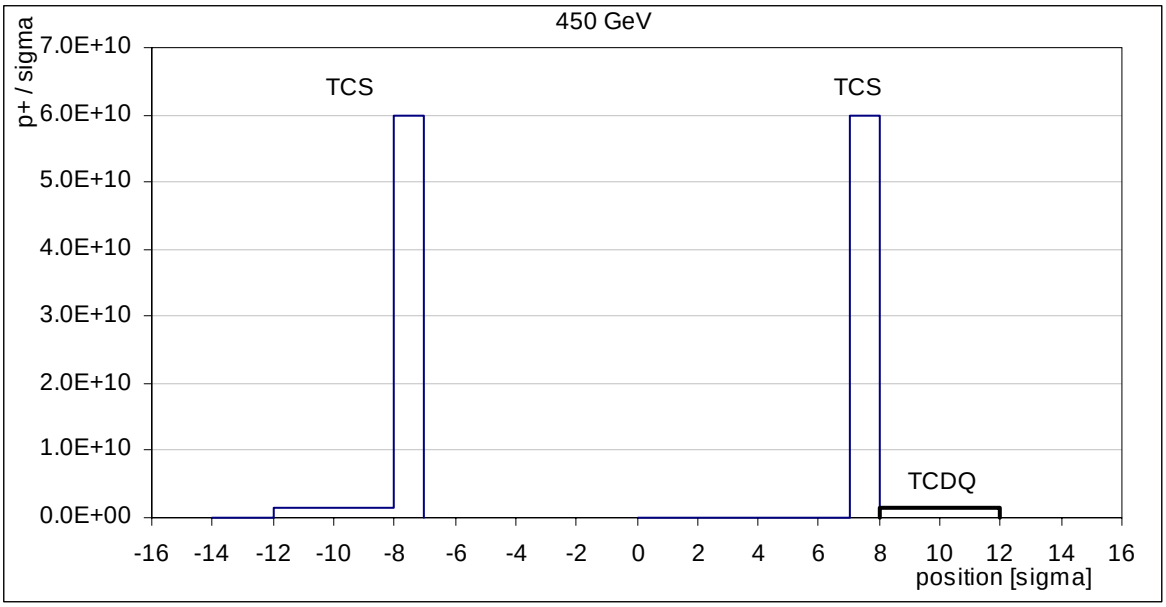

Figure 7. Assumed load distributions in p+ / sigma for 450 GeV.

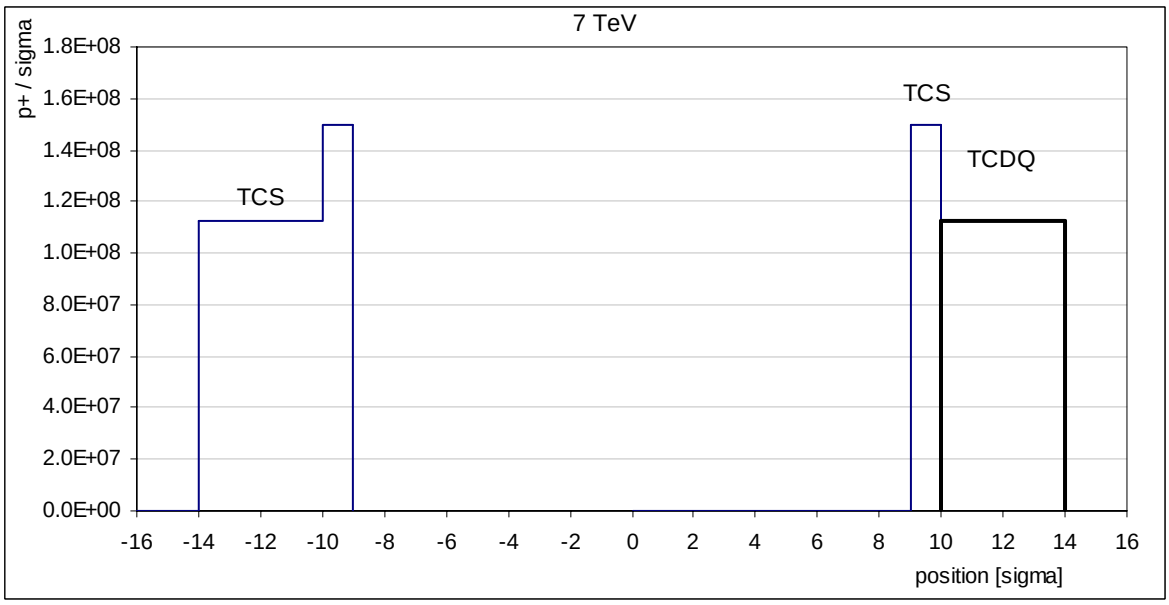

Figure 8. Assumed load distributions in p+ / sigma for 7 TeV.

3.3 Quench protection of Q4 from spurious abort gap population

During a regular beam abort, the TCDQ system will intercept any particles which are in the abort gap. This instantaneous load should not quench Q4. The maximum energy deposition in the superconducting coils should not exceed the instantaneous quench limit. This requirement places an upper limit on the spurious abort gap population [12]. As a working assumption, the impact profile is assumed to be the same as in Figure 4 (i.e bunched beam spread throughout the abort gap), with the total number of protons scaled to the total abort gap population.

3.4 Damage limits of TCDQ, TCS and TCDQM elements

The energy deposition in the TCDQ, TCS and TCDQM must not induce any damage to the protection elements themselves. For the TCDQ and TCDQM the geometry has been extensively simulated [4] and the energy deposition in the event of an asynchronous dump found to be well below the damage threshold.

4. ENERGY DEPOSITION CALCULATIONS

The FLUKA-2003 Monte-Carlo code [13] has been used to simulate particle cascades induced in the TCDQ/TCS/Q4 system in the event of an asynchronous dump and the constant load from secondary halo at 450 GeV and 7 TeV.

4.1 Particle transport and energy deposition simulation

Primary and secondary cascades induced by beam protons have been simulated. The interactions, transport and energy deposition processes were followed down to the kinetic energy threshold of 100 keV for charged particles, down to 10 keV for photons and down to 19.6 MeV for neutrons. Particles reaching or produced below these thresholds were assumed to deposit their energy locally. The energy lost by charged particles in ionisation process was converted to emitted δ-rays and thus further distributed around ionising particle tracks. Multiple Coulomb scattering was included down to the limit of Molliere's theory.

Simulated energy loss is either at a point (elastic/inelastic recoils, low energy neutron reactions) or distributed along a step (ionisation by charged particles). The calculation of energy deposition is performed mainly for neutron reactions using KERMA factors (Kinetic Energy Released in MAtter). KERMA factors give the mean energy transferred in a single neutron interaction for that neutron energy in a given material. The KERMA is then calculated by multiplying neutron fluence with the KERMA factors.

4.2 Geometry model

The TCDQ geometry described in [14] and the drawings referenced therein have been used in simulation, together with [15] and referenced drawings for the TCS geometry. Preliminary results indicated only secondary particles from TCDQ/TCS graphite and the copper cooling of TCS contribution to the Q4 loading; to minimise processing, only these elements have been simulated. Other components of the collimators have been neglected, as have the vacuum tanks.

4.3 Materials

Material compositions have been defined using atomic weight, atomic number and density. Compound materials are defined by relative atomic content. Compositions are given in Table 4.

Table 4. Material composition by relative atomic content and total material density in g/cm3 of materials used in the simulation.

		C	Cu	Fe	Al	Cr	Ni	Mn	Nb	Ti	ρ_{Total}
TCDQ	diluter	1.0	-	-	-	-	-	-	-	-	1.77
TCS	diluter	1.0	-	-	-	-	-	-	-	-	1.77
	cooling	-	1.0	-	-	-	-	-	-	-	8.96
TCDQM	all	-	-	1.0	-	-	-	-	-	-	7.87
MCBY	yoke	-	-	1.0	-	-	-	-	-	-	7.87
	shrink. cyl.	-	-	-	1.0	-	-	-	-	-	2.7
	coil	-	0.92	-	-	-	0.3	-	-	0.5	8.6
MQY	yoke	-	-	1.0	-	-	-	-	-	-	7.87
	shrink. cyl.			0.69		0.19	0.1	0.02			7.87
	coil		0.6				0.14			0.26	7.41

4.4 Statistics and biasing

In areas where simulated particle fluence is strongly attenuated, statistical precision is compromised. This is the situation in areas downstream of the TCDQM iron. Improvement may be found by employing statistical biasing to increase the multiplicity of secondaries in the affected areas. In this technique different regions are assigned relative importance (or weight) and importance sampling at regional boundaries performed on a particle-by-particle basis. The number of particles of the considered type crossing a given boundary is reduced/increased on average by a factor equal to the ratio of the importance on either side of the boundary. With the importance of a region set roughly inversely proportional to the corresponding attenuation factor the particle density is compensated and a particle density uniform in space is approached. Biasing will provide results equivalent to analogue Monte-Carlo for average quantities (such as deposited energy) in regions where purely analogue Monte-Carlo cannot.

4.5 Scoring

Meshes were defined in each element to provide energy deposition scoring (GeV/cm^3). For TCDQ and TCS Cartesian meshes covering the graphite diluters and for TCS a separate Cartesian mesh covered the copper cooling, Table 5. For magnet elements cylindrical coordinates are more convenient and a series of (r,ϕ,z) meshes were created centred on each beam-pipe, Table 6. In MCBY and MQY these may range over several material boundaries.

Table 5. Binning dimensions for Cartesian scoring meshes.

	δx (mm)	δy (mm)	δz (mm)	N_x	N_y	N_z
TCDQ	0.25	0.25	20	30	40	150
TCS graphite	0.25	0.25	20	100	320	60
copper	0.25	0.25	20	48	320	60

Table 6. Binning dimension for cylindrical scoring meshes.

	δr (mm)	$\delta \phi$ (degs)	δz (mm)	N_r	N_ϕ	N_z
TCDQM	0.50	36	46	200	10	45
MCBY	0.50	24	20	200	15	55
MQY	0.50	24	20	200	15	180

4.6 Post processing

MatLab has been used to perform off-line processing of the simulation results.

The average energy deposition (GeV/cm^3) per proton output by FLUKA-2003 was weighted by a number equivalent to the number of primary protons for each loading case. Asynchronous dump data is weighted by the product of the number of intercepting bunches and protons per bunch as given in Section 2.2.1. For beam halo data the number of protons per second is used and obtained from the secondary halo profiles shown in Figures 5 and 6 and summarised in Table 3.

Instantaneous temperature profiles have been derived from energy deposition in the adiabatic limit. A small amount of energy density *dE* deposited in a volume *dV* of a material with density ρ causes a temperature rise ΔT determined by $\Delta T = c_p \rho dV dT$. The proportionality constant c_p is the specific heat of the material. For large energy deposits the specific heat can no longer be considered constant, and its temperature dependence must be considered. The specific heat $c_p(T)$ for graphite and copper are given by Eq. 1 and Eq. 2 while that of iron is considered constant at 0.44 J/g°C over the expected range of temperature.

$$c_p^{graph}(T) = 528.75 - 205.9T^{1/3} + 154.21T^{1/2} - 1.53T + 9.15\times10^{-5}T^2 \qquad \text{(Eq. 1)}$$

$$c_p^{Cu}(T) = 381.12 + 0.16T - 1.09\times10^{-4}T^2 \qquad \text{(Eq. 2)}$$

Now ΔT can be extracted from :

$$\frac{dE}{dV} = \rho\int_{T_0}^{T_0+\Delta T} c_p(T)dT \qquad \text{(Eq. 3)}$$

by solving numerically the upper limit of the integral.

5. ENERGY DEPOSITION RESULTS AND DISCUSSION

5.1 Asynchronous dump

Deposition and temperature profiles during an asynchronous dump are shown in Figures 9 to 15. The profiles in each coordinate intersect the point of maximum load in each of the elements and are in the adiabatic limit. The maximum depositions, maximum temperature load to graphite and maximum energy flow out of the magnets are summarised in Table 7. A qualitative précis of the main observations follows.

The TCDQ is seen to absorb the majority of energy from showers initiated by protons impinging its surface. Minimal shower leakage is observed out of the rear surface.

The TCS is exposed to the small number of secondary particles escaping TCDQ but also two proton bunches that impinge directly on its volume. Naturally direct impacts dominate loading, as indicated by the peak at inner edge of the right-hand diluter. This creates a highly localised (*x*,*y*) peak in the temperature profile at ~800 °C. Because we are far from the depth of the shower maximum the temperature rise is seen to continue approximately linearly to its reach maximum at the rear face of the graphite volume.

The 120 cm TCS length is insufficient to contain the showers created by direct impacts (shower max ~150 cm) and punch-through occurs. Due to this punch-through, the energetic particle fluence leaving TCS is strongly peaked at low (x,y). However these particles pass through the TCDQM aperture and continue downstream with no effect. This means that downstream elements are affected only by low energy particles in the tail of the TCS distributions and experience a minimal load.

Loading to the MQY is greater than that of the more forward MCBY. This effect is attributed to cascade particles that scatter out of the upstream volumes and are then swept off axis by the MCBY magnetic fields impacting directly on the MQY internal surface.

Table 7. Summary of instantaneous load due to asynchronous dump at 7 TeV.

	peak load (J/cm^3)	**ΔT (K)**	**Energy flow (J)**
TCDQ (front)	2139	712	-
TCS (right)	2283	679	-
TCDQM	44.5	12.8	-
MCBY	26.2	-	262
MQY	38.0	-	1836

5.2 7 TeV secondary halo

Energy deposition and temperature profiles during one second of secondary halo load at 7 TeV are shown in Figures 16 to 22. The plots follow profiles that intersect the point of maximum load. Loading is integrated over one second and therefore energy densities (J/cm^3) can be regarded as power densities in W/cm^3. The maximum depositions, maximum temperature load to graphite and maximum energy flow out of the magnets are summarised in Table 8. A qualitative précis of the main observations follows.

Shower maximum in the TCDQ graphite is again found at a point approximately 150 cm into the front diluter block. Loading to the rear block is a factor 10 lower than that in the upstream volume since it is exposed only to the secondary particles found in the tail of the shower distribution from the forward block.

The TCS loading is asymmetrical. The right-hand jaw is largely protected by TCDQ and experiences comparatively reduced. In both cases loading is localised in the first centimetre from the innermost edge.

Being protected by TCS, the peak loading to downstream elements are an order of magnitude lower but continue to display the same left-right asymmetry. As for the asynchronous dump case the loading to MQY is enhanced by the bending of cascade particles originating in upstream elements by the MCBY dipole field.

Table 8 Summary of load in one second due to secondary beam halo at 7 TeV.

	Peak load J/cm3	**ΔT (K)**	**Energy flow (J)**
TCDQ (front)	0.73	0.30	-
TCS (left)	0.59	0.25	-
TCDQM	0.029	0.008	-
MCBY	0.017	-	0.154
MQY	0.024	-	0.985

5.3 450 GeV secondary halo

Energy deposition and temperature profiles for one second of load from secondary halo at 450 GeV are shown in Figures 23 to 29. The plotted data follow profiles that intersect the point of maximum load in each of the elements. Again halo loading is integrated over one second and therefore energy densities (J/cm^3) can be interpreted as power densities in W/cm^3. The maximum depositions, maximum temperature load to graphite and maximum energy flow out of the magnets are summarised in Table 9. A qualitative précis of the main observations follows.

At 450 GeV the fraction of protons in the halo beyond 8σ is small. Therefore the TCDQ experiences minimal loading and the protection offered by TCDQ to the TCS right-hand jaw has little effect and the energy deposition profiles for the left-hand and right-hand sides of TCS are essentially symmetrical. In both the left-hand and right-hand jaws the majority of energy is deposited within 5 mm of the inner edge.

Again the protection offered by TCS means the peak loading to downstream elements are an order of magnitude lower. Once more the loading to the MQY is enhanced compared to that of MCBY by the bending of cascade particles scattering out of the graphite volumes by the MCBY dipole field and impinging the inner surface of the beam-pipe aperture.

Table 9 Summary of load in one second due to secondary halo at 450 GeV

	Peak load J/cm3	**ΔT (K)**	**Energy flow (J)**
TCDQ (front)	0.13	0.057	-
TCS (left)	2.4	0.98	-
TCDQM	0.33	0.097	-
MCBY	0.12	-	1.50
MQY	0.12	-	2.33

Figure 9. 7 TeV asynchronous dump load to TCDQ

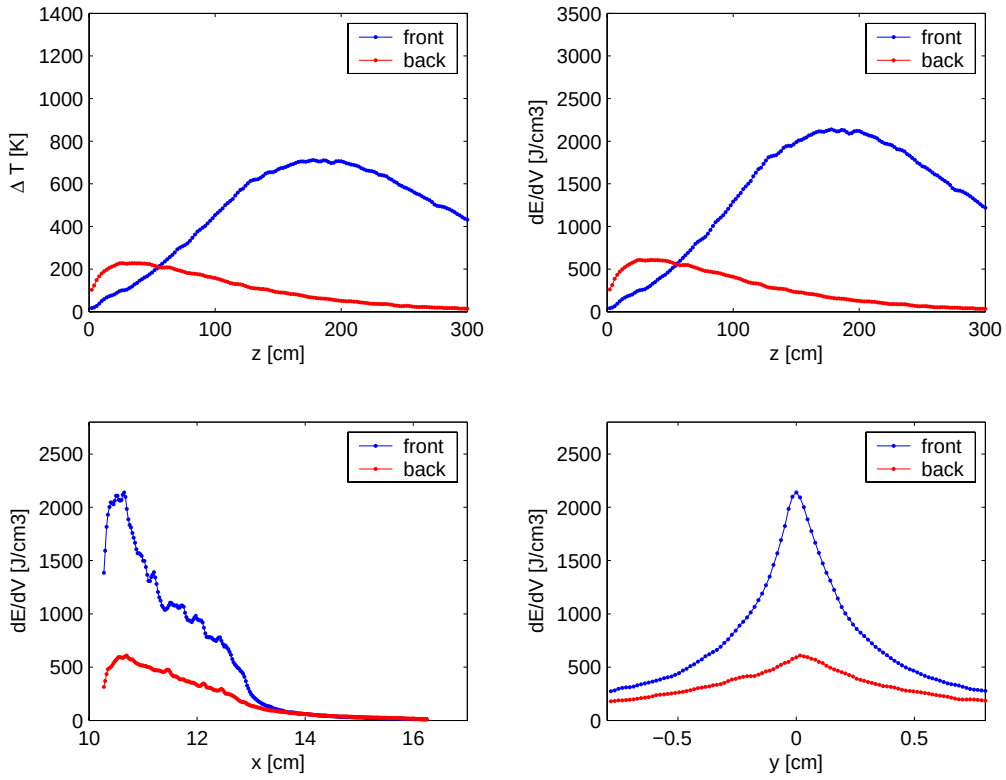

Figure 10. 7 TeV asynchronous dump load to TCS

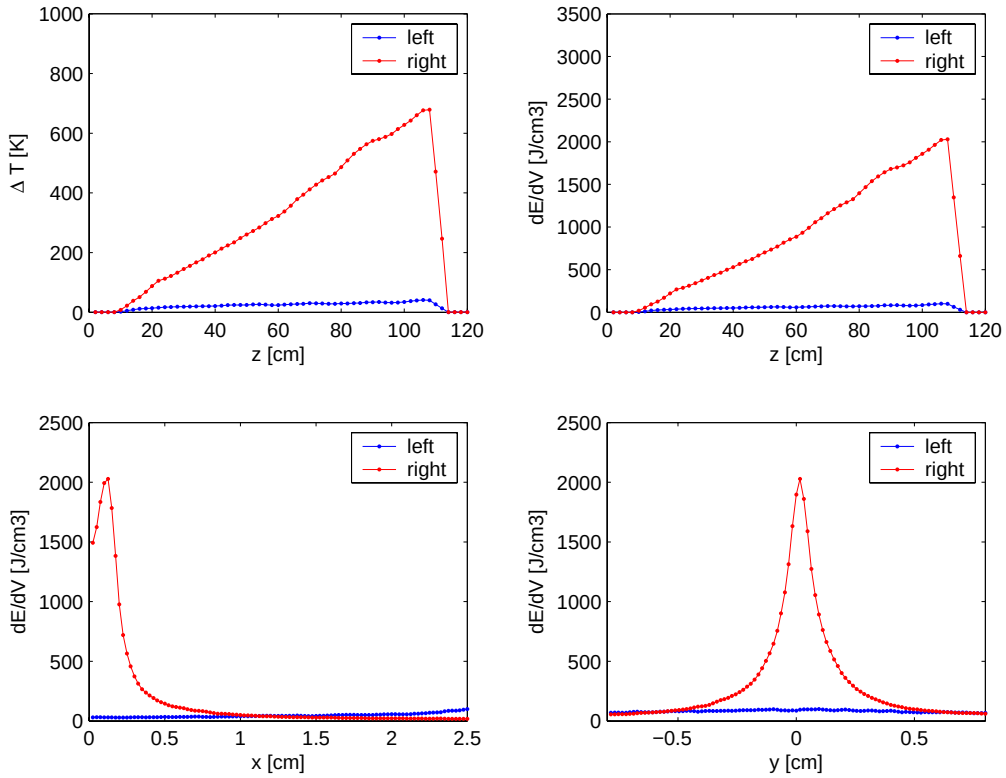

Figure 11. 7 TeV asynchronous dump load to TCDQM

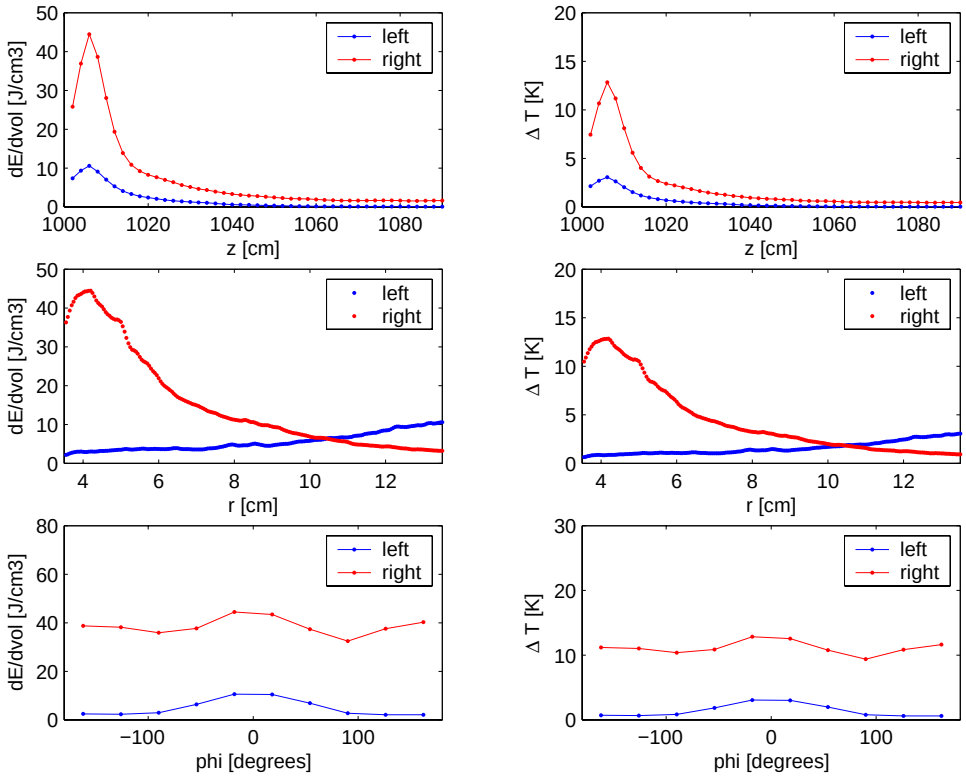

Figure 12. 7 TeV asynchronous dump load to MCBY

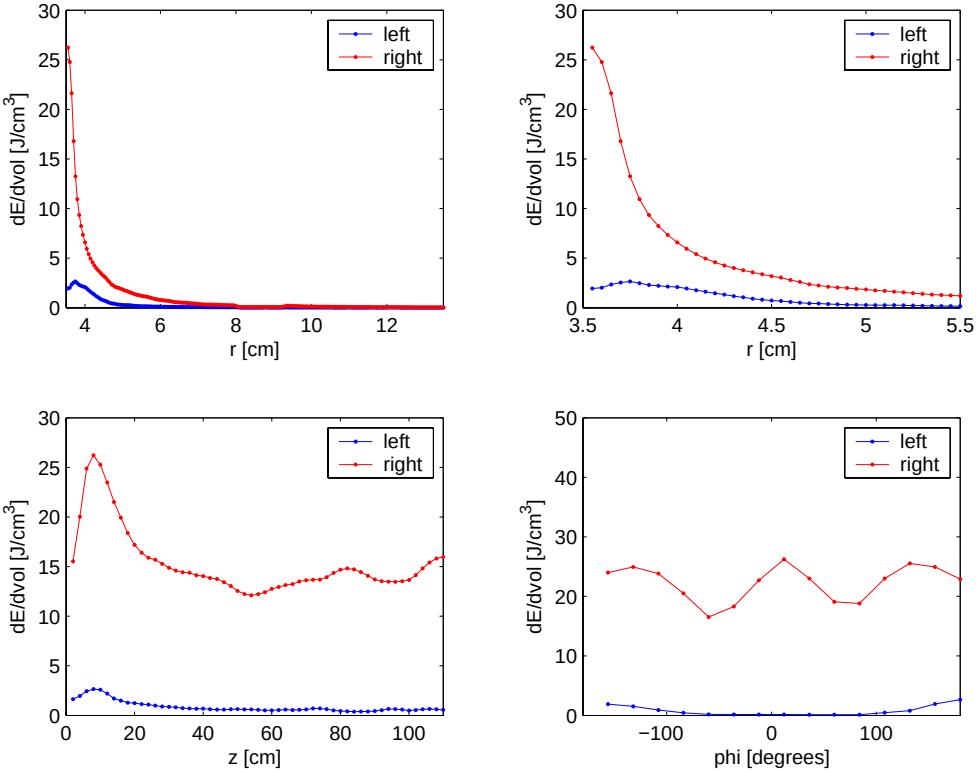

Figure 13. 7 TeV asynchronous dump load to MQY

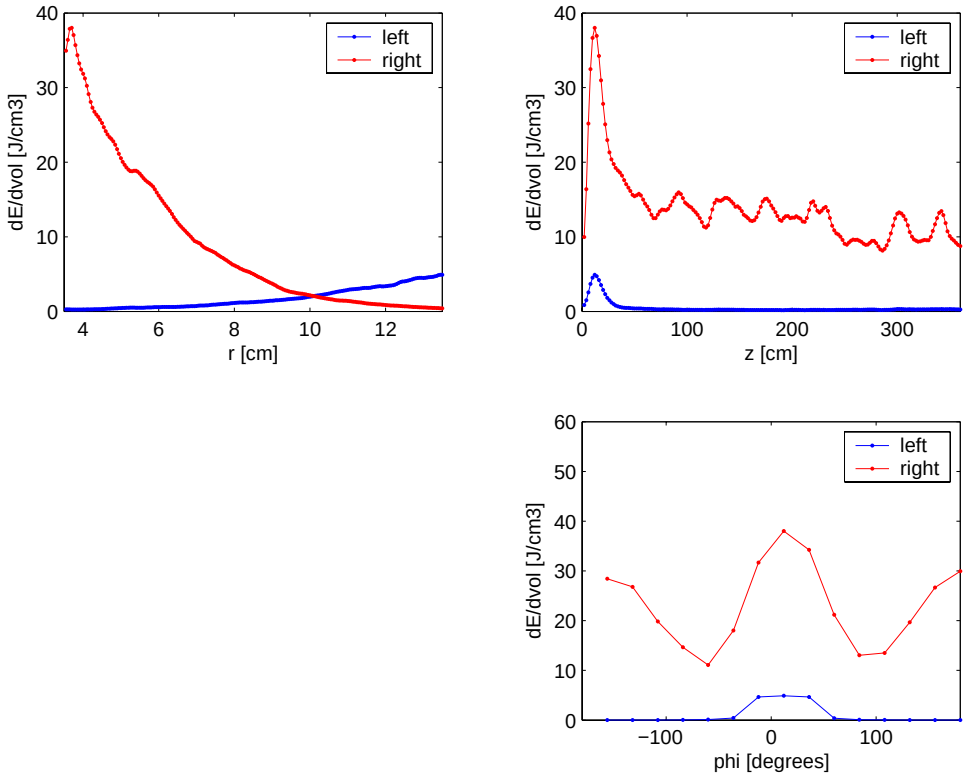

Figure 14. Max energy flow in MCBY due to 7 TeV asynchronous dump

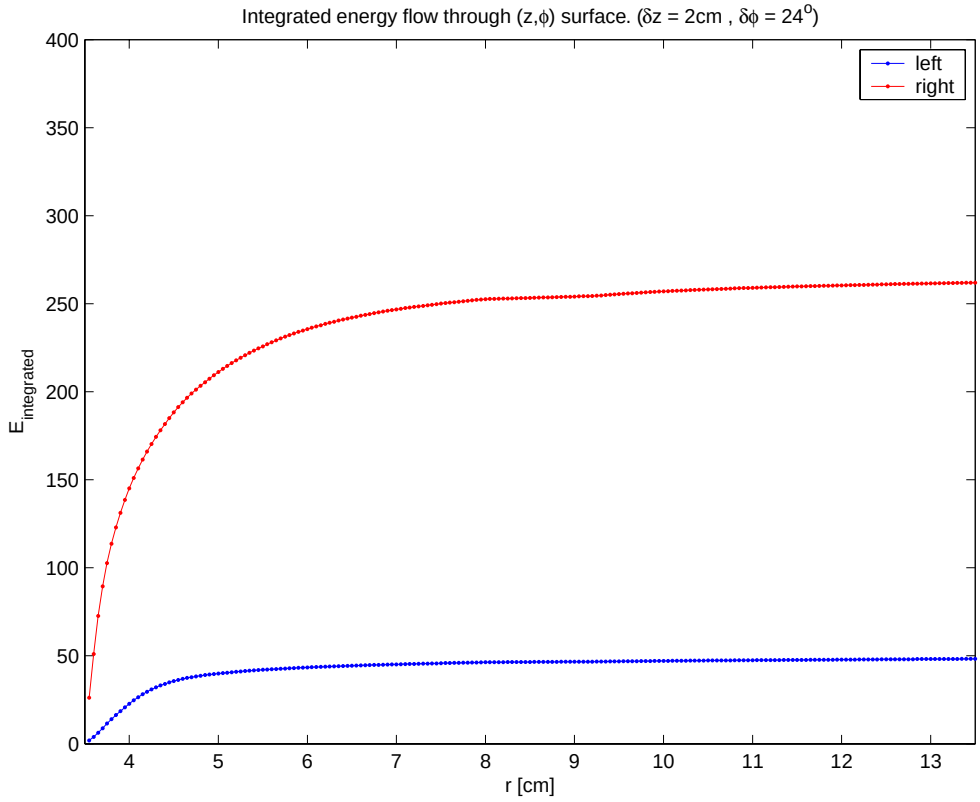

Figure 15. Max energy flow in MQY due to 7 TeV asynchronous dump

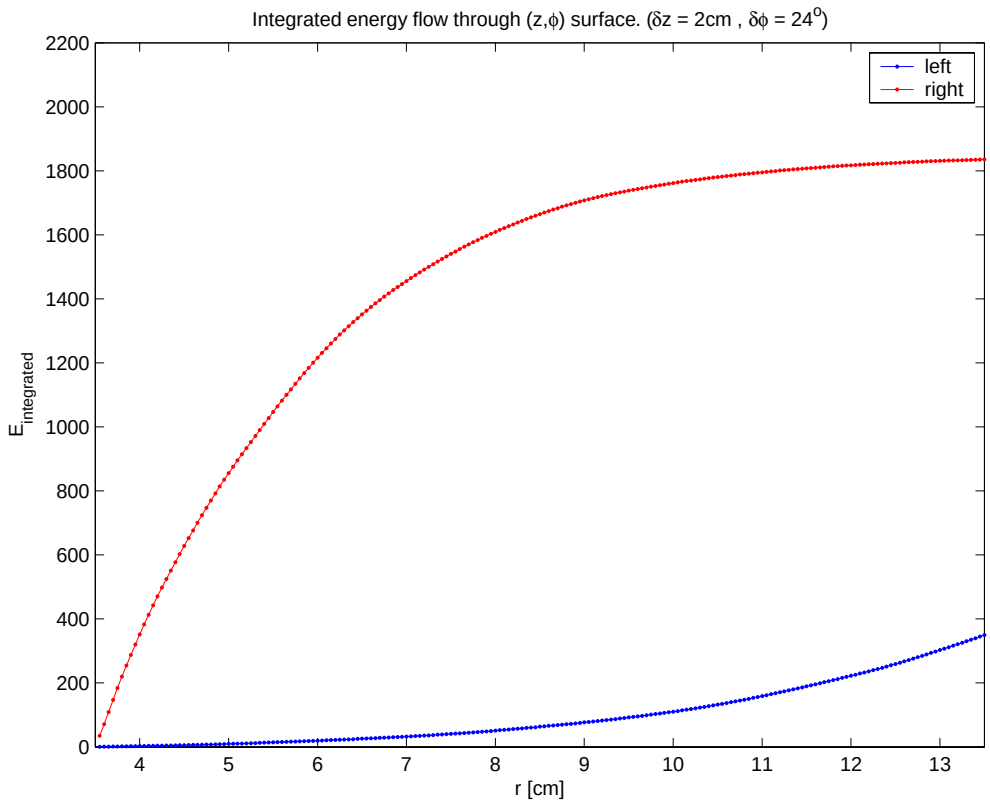

Figure 16. 7 TeV halo load to TCDQ

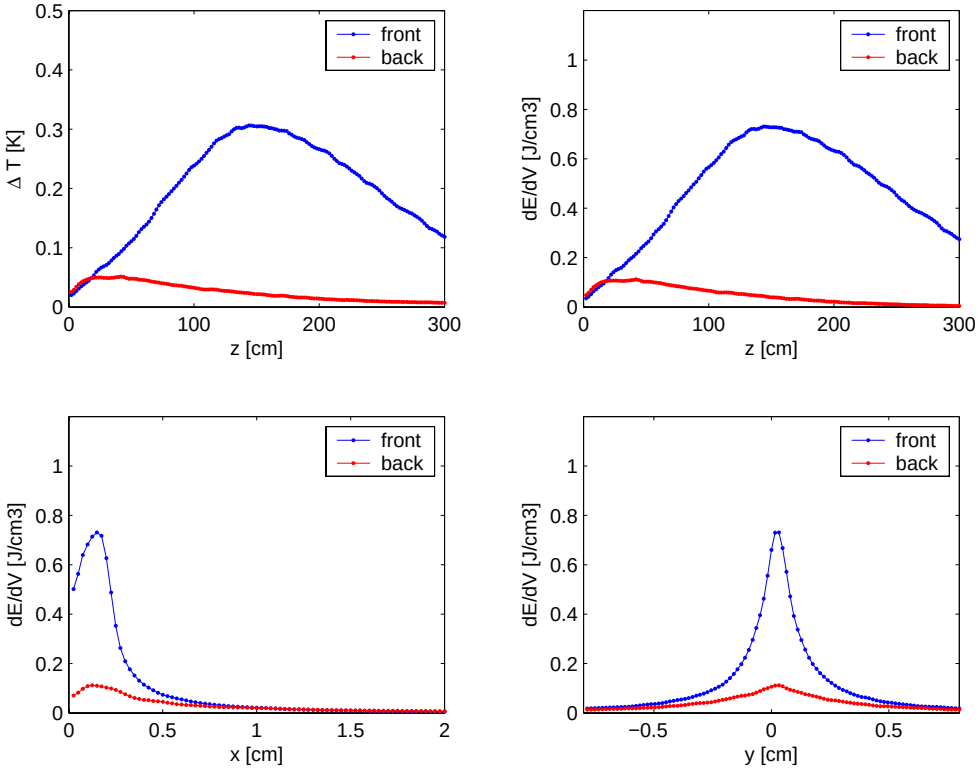

Figure 17 7 TeV halo load to TCS

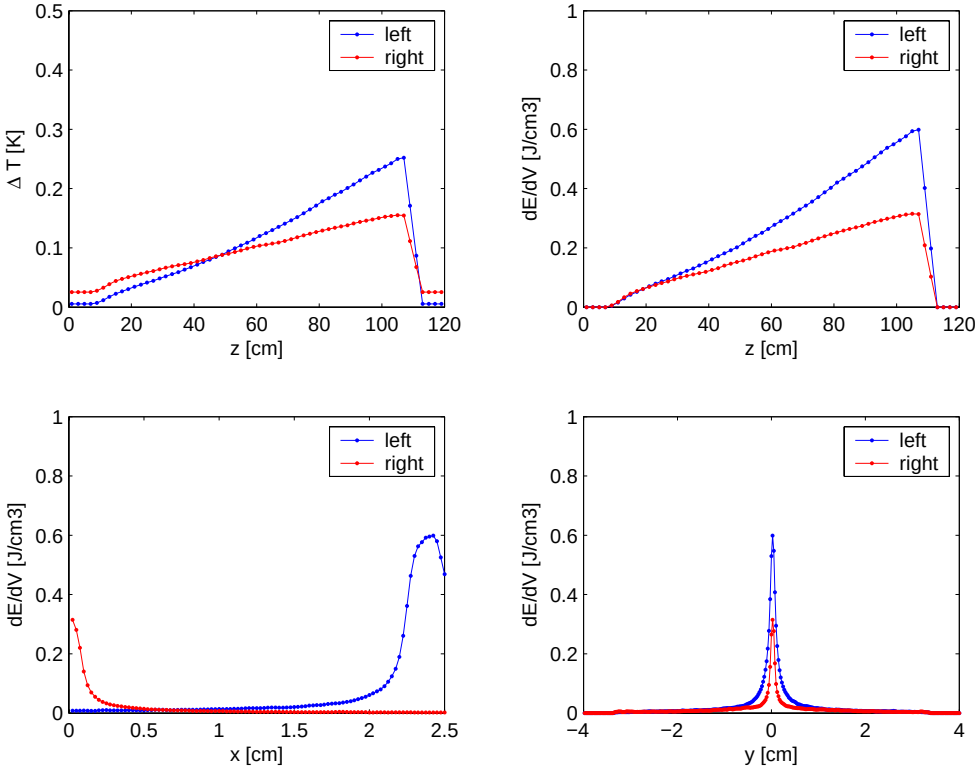

Figure 18. 7 TeV halo load to TCDQM

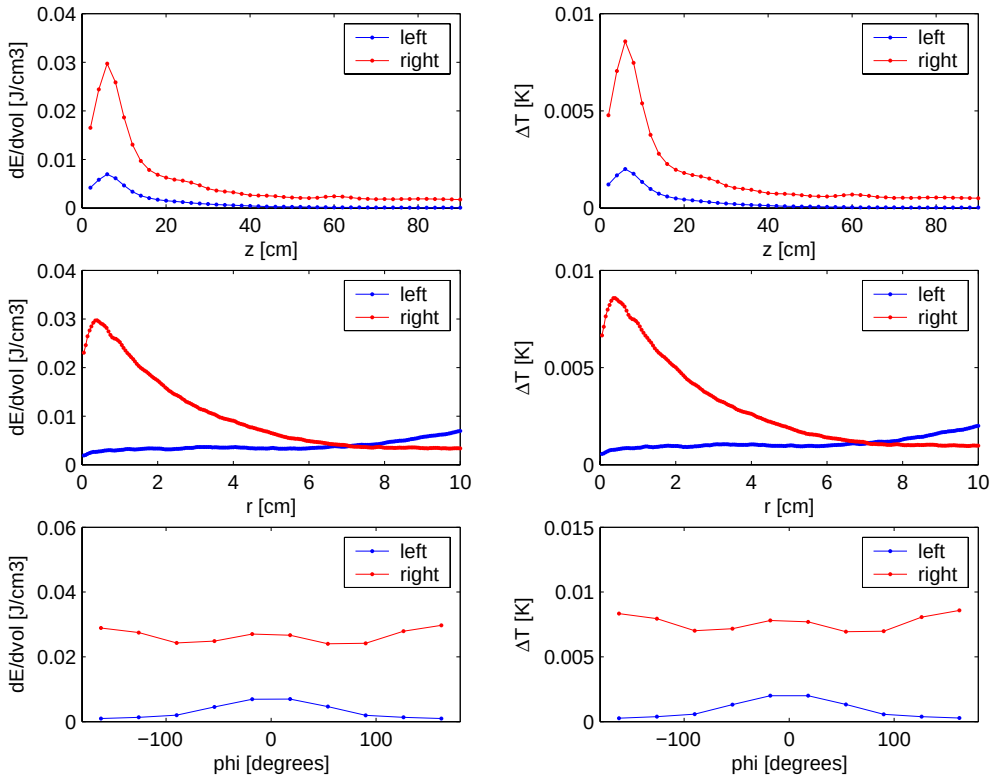

Figure 19. 7 TeV halo load to MCBY

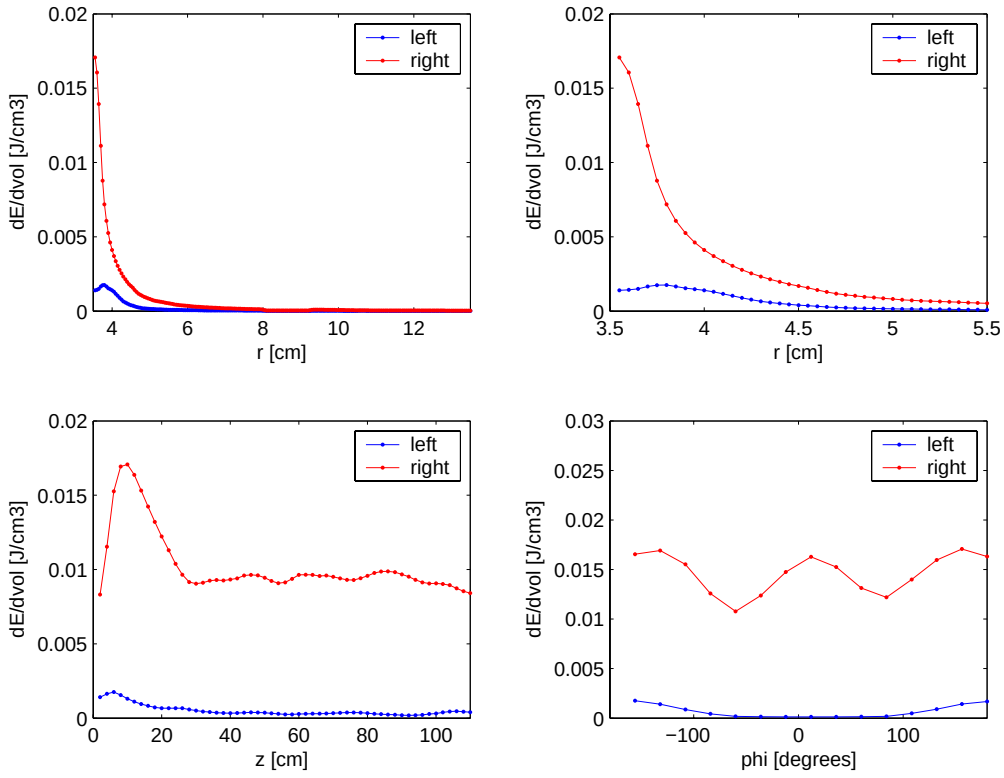

Figure 20. 7 TeV halo load MQY

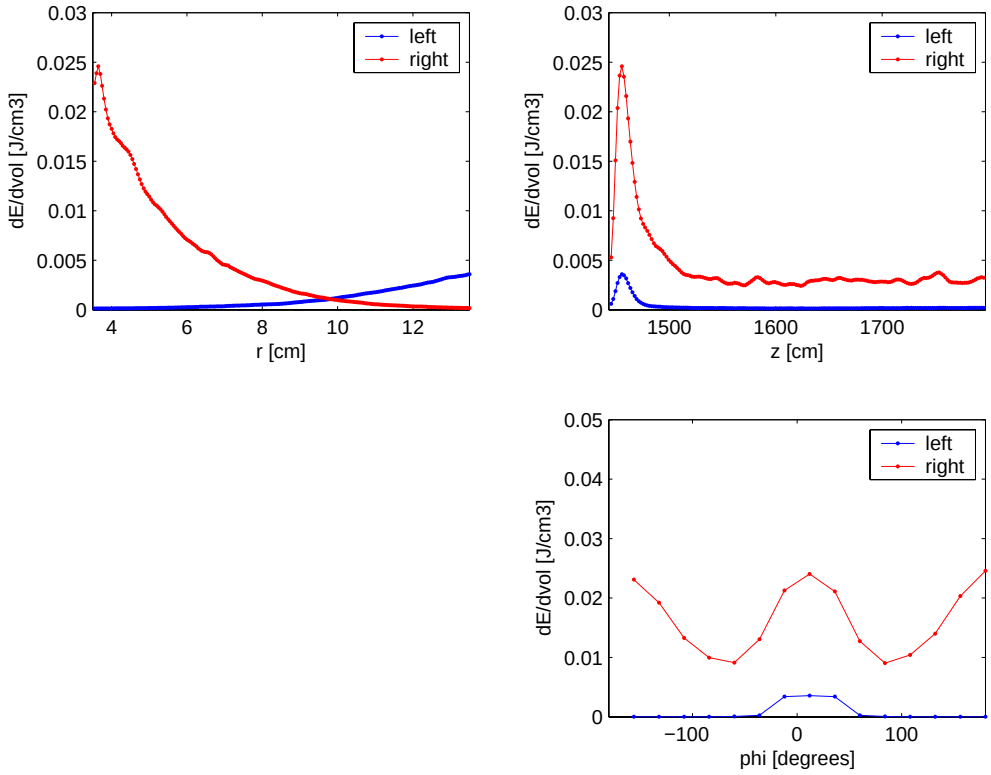

Figure 21. 7 TeV secondary halo max energy flow in MCBY

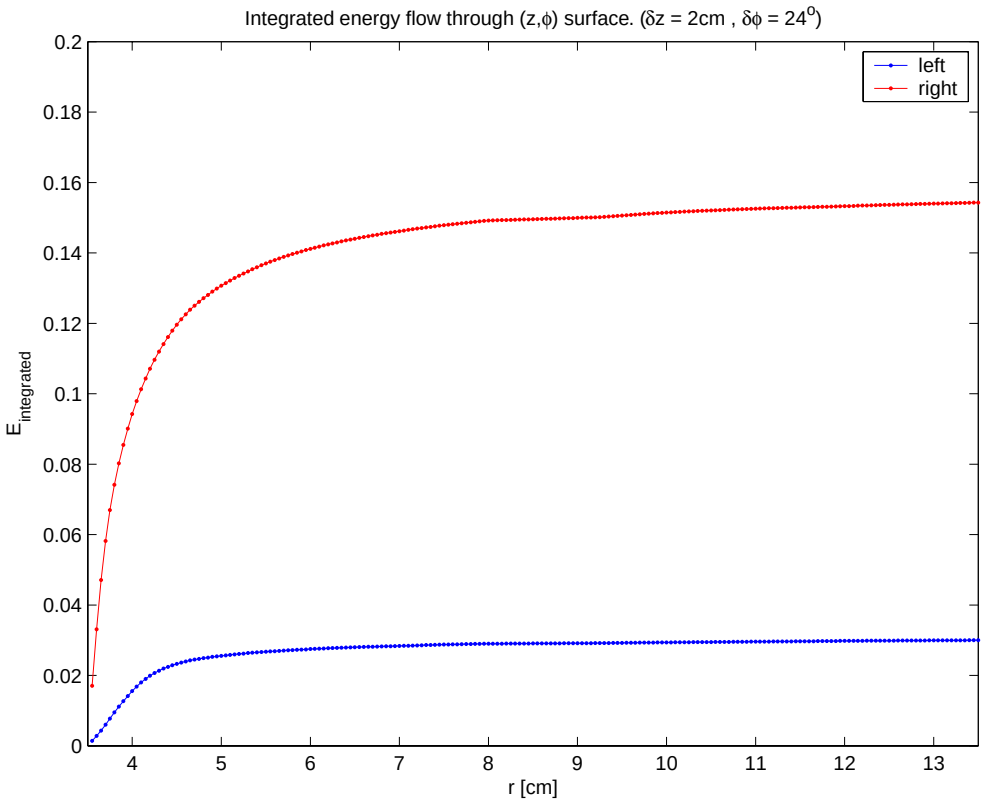

Figure 22. 7 TeV secondary halo max energy flow in MQY

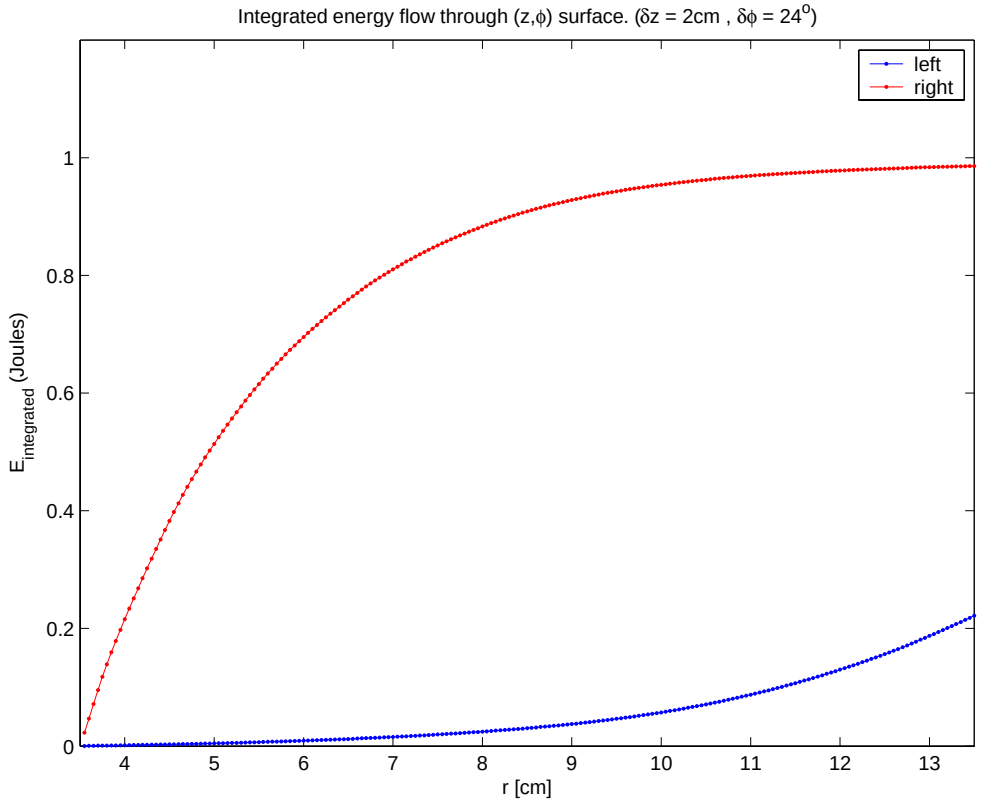

Figure 23. 450 GeV halo load to TCDQ

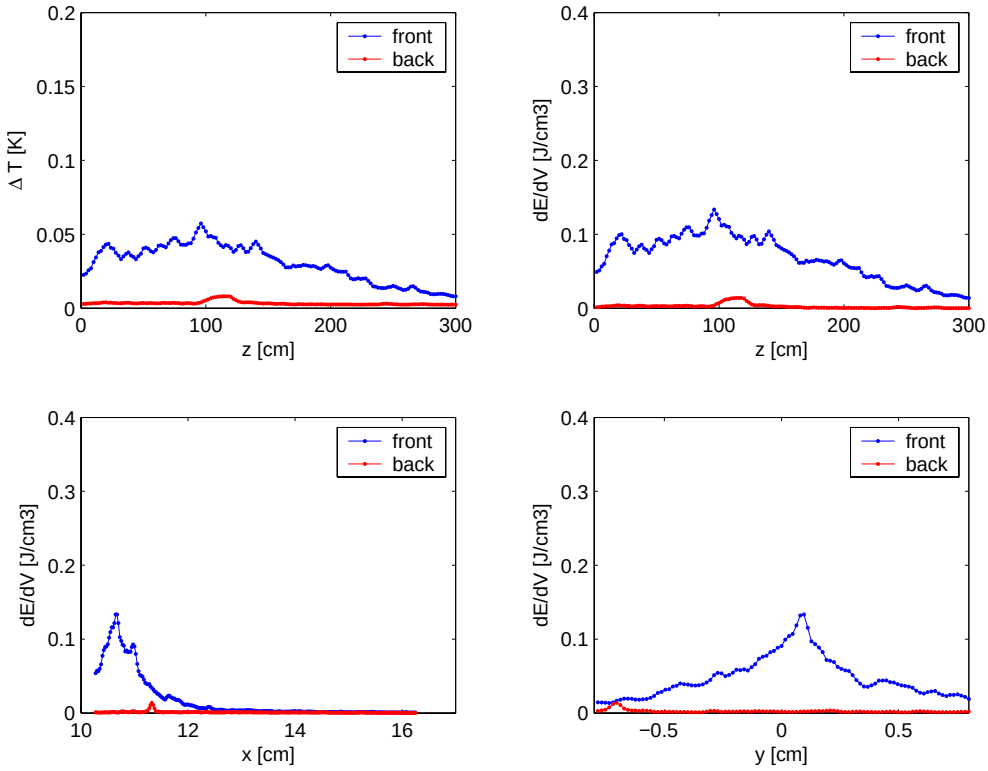

Figure 24. 450 GeV halo load to TCS

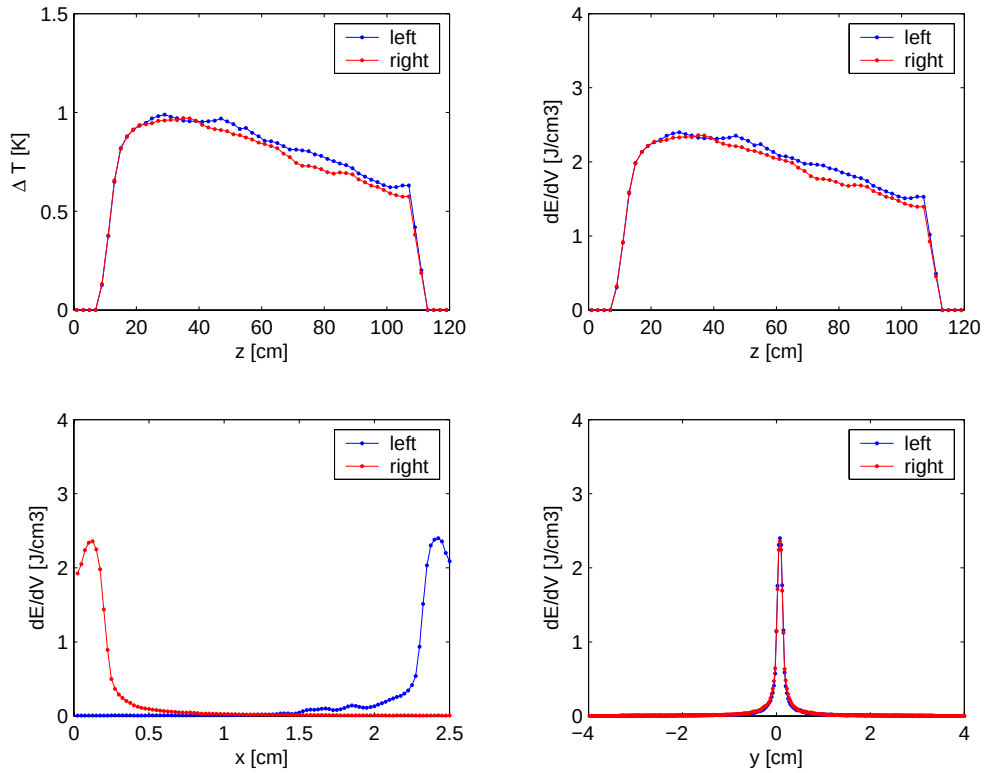

Figure 25. 450 GeV halo load to TCDQM

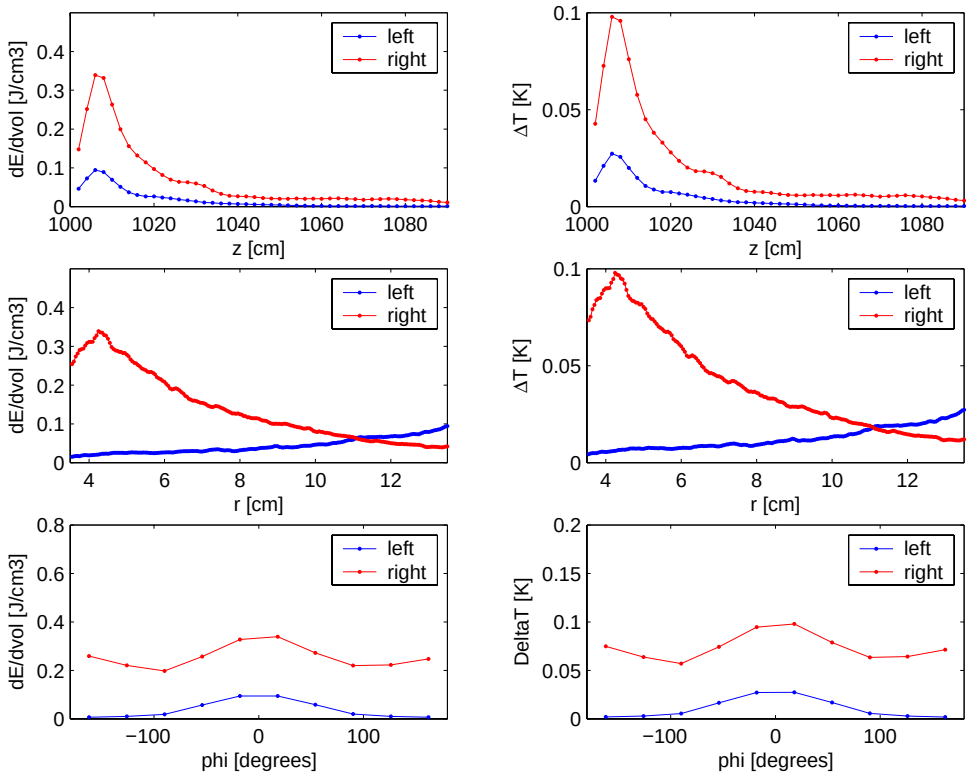

Figure 26. 450 GeV halo load to MCBY

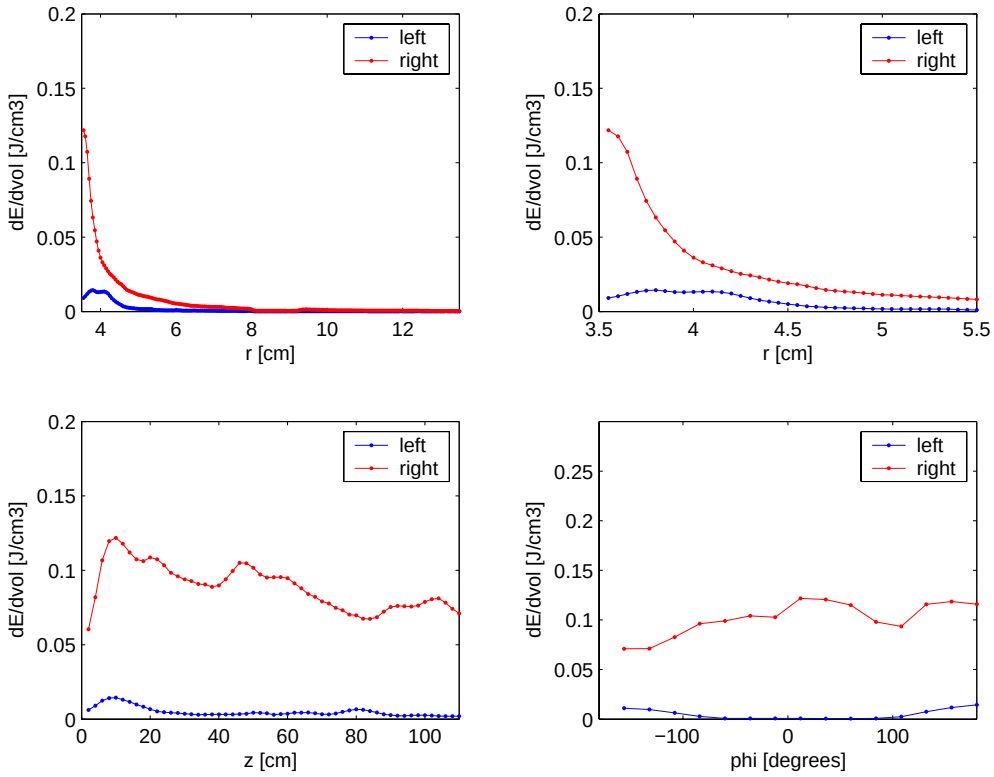

Figure 27. 450 GeV halo load to MQY

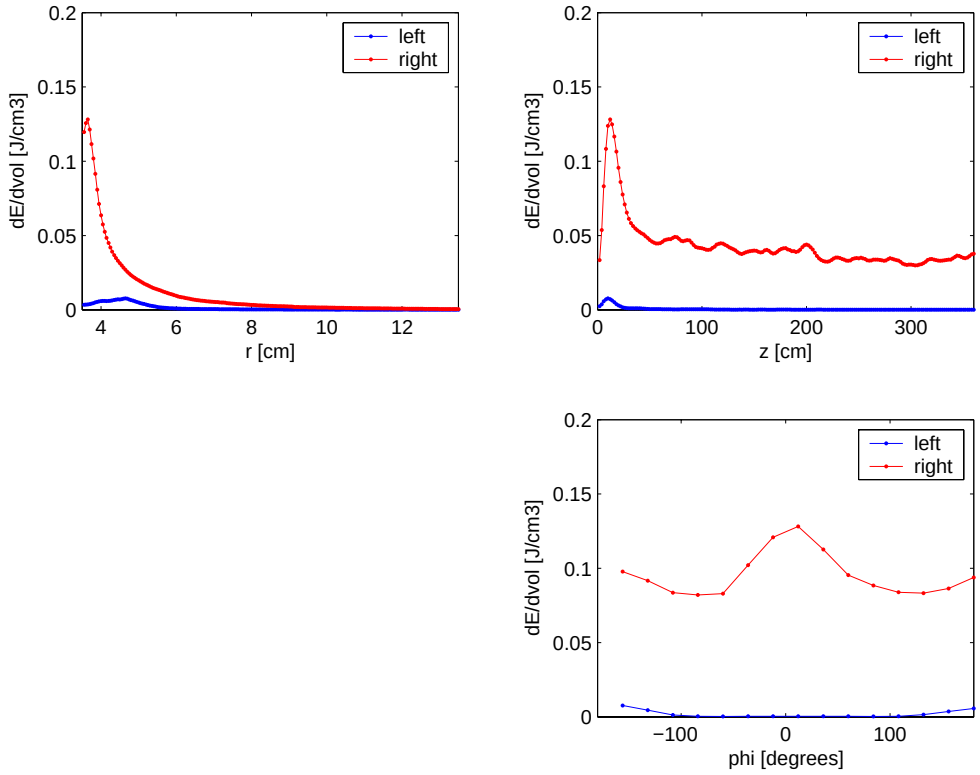

Figure 28. 450 GeV secondary halo max energy flow in MCBY

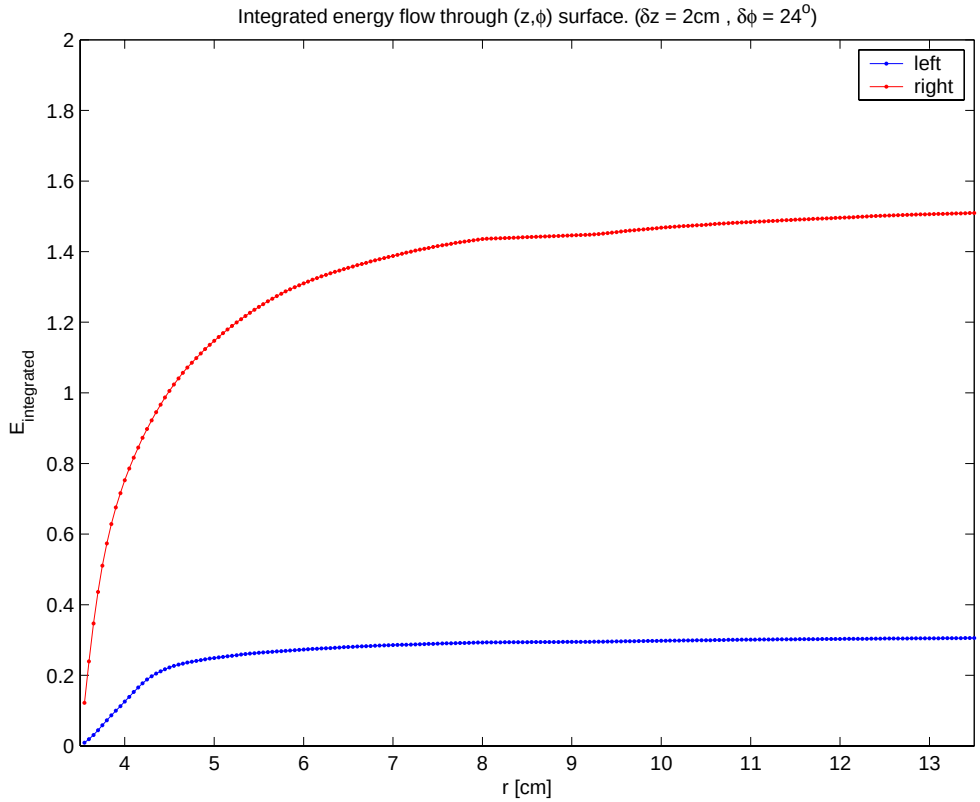

Figure 29. 450 GeV secondary halo max energy flow in MQY

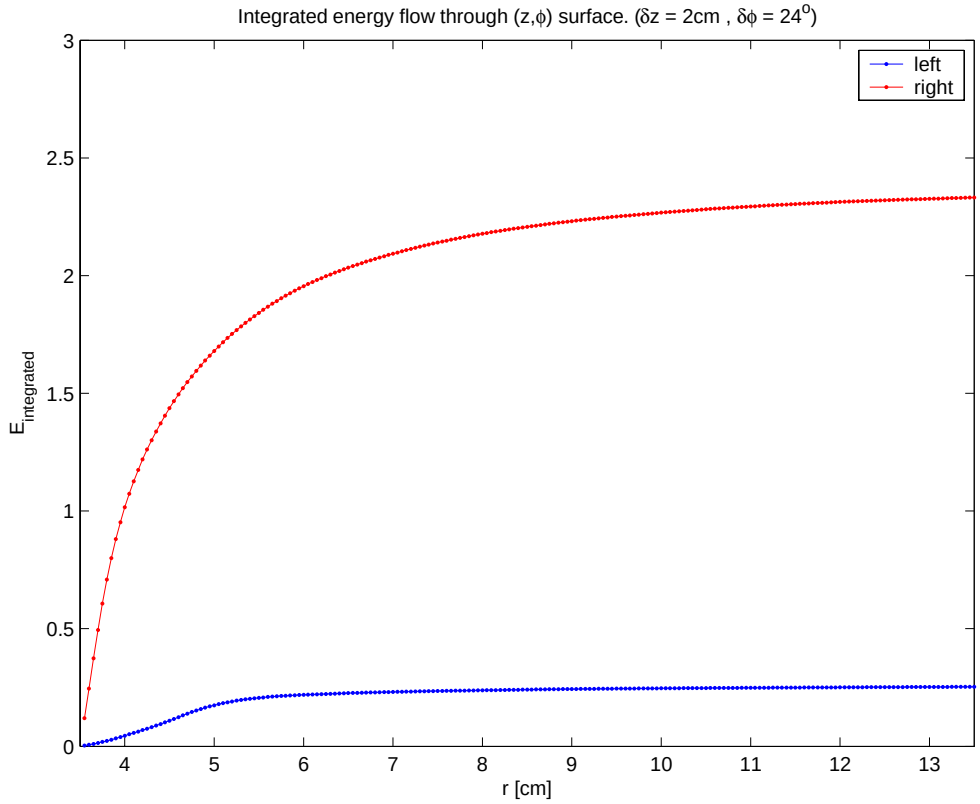

6. SUMMARY, IMPLICATIONS AND FUTURE WORK

6.1 Protection against asynchronous dump

The TCS/TCDQ/TCDQM system fulfils its primary design objective of protecting the Q4 magnet, the LHC arc and the LHC inner triplet from destruction in the event of an asynchronous beam dump, up to LHC ultimate intensity. The energy deposition in the Q4 and the protection elements themselves are all within acceptable limits.

An important condition that this system operates correctly is that the beam position relative to the TCDQ/TCS be maintained to within 0.5 σ.

6.2 Prevention of quench from abort gap population in the event of a normal dump

The results show that 40 J/cm^3 are deposited in the MQY coil, with the ultimate bunch intensity of 1.7 10^{11} p+ (2 10^{10} p+ / m). Assuming the quench limit is 4 mJ / cm^3, the maximum abort gap population which can be tolerated at 7 TeV corresponds to 1.7 10^7 p+ / bunch (2 10^6 p+ / m).

At 450 GeV the corresponding limit in abort gap population will be at least two orders of magnitude higher due to the higher quench limit in the MQY and the increased stopping power of the TCDQ; limits of 2 10^9 p+ / bunch (2 10^8 p+ /m) are assumed.

These figures are lower than the previously assumed limits, which were 1.1 10^6 p+ /m at 7 TeV and 10^9 p+ / m at 450 GeV [12]. This may have important consequences both for the abort gap monitoring and abort gap cleaning systems currently planned for the LHC, since according to [12], at 450 GeV in the absence of abort gap cleaning, 5 % capture losses can populate the abort gap to this density, and the longitudinal lower lifetime limits increase to about 80 h and 1 h at 7 TeV and 450 GeV respectively. In particular, the 450 GeV case should be simulated explicitly with FLUKA to refine the estimate given above, to provide a real limit.

6.3 Prevention of quench from halo particles during low beam lifetime

The results show that at 450 GeV the maximum power deposited in Q4 is around 120 mW/cm^3, with a total power in the magnet of about 2.3 W. For 7 TeV the corresponding figures are 24 mW/ cm^3 and 1 W, respectively.

The limit on the total power deposited is assumed to be 34 W at all energies; here the situation appears to be comfortable.

However, for the localised DC power, the assumed limits are in the range 1-10 mW/cm^3 at 450 GeV and 0.2-5 mW/cm^3 at 7 TeV. The simulations with the assumptions detailed above show power depositions a factor of 12-120 and 5-100 higher than these limits, at 450 GeV and 7 TeV respectively.

These preliminary results show already that the power deposited in the Q4 magnet during low beam lifetime will be a serious concern for LHC operation, and if these figures cannot be improved, might even limit the total beam intensity unless extra measures are taken. A factor of at least 10, and preferably 100, improvement in the peak deposited DC power is required at both injection and top energy.

There are several potential areas to be addressed for improvement:

- The TCDQM aperture in the present simulations was originally conceived with a diameter of 70 mm, as for the MQY coil, for simplicity of construction. In view of the results described above, it has already been decided that the actual TCDQM will be constructed in vacuum, with a profile adapted to the aperture of the beam screen in the MQY magnet. The mask will have a diameter of around 56 mm. This will reduce the energy deposition in the MQY; the improvement must be simulated and quantified in FLUKA with an updated geometry.

- In the simulations described above, the magnet cold-bore and the beam screen and transition pieces were not included. In fact these will intercept the secondary particles escaping the TCS/TCDQ/TCDQM before the superconducting coil, and because of the grazing incidence angles will reduce the energy deposited in the coil. Again, this more exact geometry must be simulated in FLUKA to be able to quantify the improvement.

- The secondary halo shape assumed in 3.2 does not take into account any losses on the LHC aperture between the collimation sections and IR6. Studies are ongoing [9], and it is expected that the results will show an improvement in the loss profile at the large amplitudes concerned, especially at 450 GeV.

- The settings of the TCS/TCDQ can be relaxed at 450 GeV, since at this energy the damage limit corresponds to about 12 bunches [16], which means that the protection system aperture can be relaxed by several sigma, since in principle there will not be any damage to the LHC arc even if some bunches are allowed through with amplitudes above 7.5 σ. From Figure 5, it can be seen that opening the system aperture by only 1 σ reduces the secondary halo by almost a factor of 10; it seems that a **factor 10** improvement is easily possible at 450 GeV by relaxing the settings. At 7 TeV the situation is different, since the damage level is below one bunch and the system must ensure that no bunches are allowed through at larger amplitudes.

- The magnet quench limits values quoted are not specific to the MQY, and there is the possibility that these might change if more detailed information is available for this specific case. A full study would involve producing a 3-d energy deposition map with FLUKA, and then analysing this with dedicated tools to determine the quench limits for the particular magnet. The CERN workshop on quench and damage limits to be held in March 2005 should address some of these issues.

- Relaxing the design constraint to only be compatible with LHC nominal bunch intensity instead of LHC ultimate brings a **factor of 1.5** improvement at 450 GeV and 7 TeV. The system would need upgrading to work with ultimate beam intensity.

Taking all the above into account, and compared to the numbers presented above, it appears that a **factor 15** improvement can easily be obtained at 450 GeV, by assuming nominal beam with the TCS/TCDQ settings relaxed by about 1 σ. The detailed halo tracking, improved TCDQM geometry and beam screen effect will bring an additional improvement, but are still to quantify.

At 7 TeV the situation is more critical, since it will be difficult or impossible to relax the settings. Here it is essential that the study be completed to quantify the above effects. It appears that continued refinement may provide the reassurance that the LHC can be operated with the

specified lifetimes, without provoking quenches in Q4 due to scattering from the TCS/TCDQ. This, however, remains to be demonstrated.

6.4 Future work

The results obtained with respect to the primary design function of the TCS/TCDQ system confirm that the system operates correctly in this respect, without damage to the new TCS element.

However, the quench aspects with the secondary halo give cause for serious concern, especially at 7 TeV where the high damage potential of even a single bunch means that it probably will not be possible to relax the settings of the TCS/TCDQ system.

In view of these results, and also because of the reduced limit which has now been placed on the abort gap population, the present FLUKA study and the related halo and failure case studies must be extended and completed with high priority:

- The FLUKA study needs to be completed with the new TCDQM profile and the addition of the beam screen and cold bore to the MQY geometry.

- The quench limits in the MQY magnet should be revised with the magnet builders, and if necessary a 3-d map of the energy deposition used to better defined quench limits.

- The realistic secondary halo should be simulated at the TCDQ, by tracking with many seeds through the LHC with realistic errors, apertures, collimator settings and orbits.

- The sensitivity of the protection levels to the TCS/TCDQ positioning should be determined by particle tracking, to see to what extent the settings can be relaxed for different machine energies and modes.

- The 450 GeV case for an asynchronous dump should be simulated with the refined geometry, to enable the limits to be derived for the tolerable abort gap population at this energy. The 7 TeV case should also be redone to check the effects of the updated geometry.

7. ACKNOWLEDGEMENT

The work described in this note has benefited greatly from the efforts and input of B.Jeanneret, R.van Weelderen, W.Weterings and R.Assmann.

8. REFERENCES

[1] O. Brüning et al., “LHC Design Report Volume I - the LHC Main Ring”, CERN-2004-003, 2004.

[2] W.Weterings, B.Goddard, “TCDQ Collimator to Protect the LHC against Unsynchronised Beam Dumps”, LHC-TCDQ-ES-0001-00-10, EDMS 503490, 2005.

[3] R.Assmann et al., “The Consequences of Abnormal Beam Dump Actions on the LHC Collimation System”, LHC-Project-Note-293, 2002.

[4] M.Sans Merce, “Simulations of Energy Deposition in the TCDQ Collimator”, CERN EDMS 458438 v.1, 2004.

[5] O. Brüning, B. Jeanneret, "Optics Constrains Imposed by the Injection in IR2 and IR8", LHC Project Note 141, May 1998.

[6] A.Drozhdin et al., “Protecting LHC Components Against Radiation Resulting From an Unsynchronized Beam Abort”, CERN, LHC-Project-Report-478, 2001.

[7] B.Jeanneret, “Quench Levels and Transient Beam Losses in LHC Magnets”, CERN-LHC-Project-Report-44, 1996.

[8] R. van Weelderen, Private Communication 2004.

[9] S.Raedelli, “LHC Aperture and Commissioning of the Collimation System, Second LHC Project Workshop, Chamonix XIV, 2005.

[10] V.Kain et al., “Attenuation and Emittance Growth of 450 GeV and 7 TeV Proton Beams in low-Z Absorber Elements”, EPAC ’04, 9th European Particle Accelerator Conference 2004.

[11] R.Assmann, Private Communication 2004.

[12] S.Fartoukh, B.Jeanneret, E.Shaposhnikova, “LHC Abort Gap Filling by Proton Beam”, CERN LHC Project Report 763, 2004.

[13] A.Fasso, A.Ferrari, J.Ranft, P.R.Sala, "FLUKA: Status and Prospective for Hadronic Applications", Proc. MonteCarlo 2000 Conference, Lisbon, Springer-Verlag Berlin, pp.955-960, 2001.

[14] W.Weterings, B.Goddard, “TCDQ Layout and Dimensions”, LHC-TCDQ-EC-001, CERN EDMS 503480, 2004.

[15] CERN CDD, LHCTCS_P0079.

[16] V.Kain, “Damage Levels: Comparison of Experiment and Simulation”, Second LHC Project Workshop, Chamonix XIV, 2005.